Implementation of a Cohesive Crack Model in Grain-based DEM Technique for Simulating Fracture in Quasi-Brittle Geomaterial

GEOQuébec 2015
Challenges from North to South
Des défis du Nord au Sud

Farahmand K. & Diederichs M.S.
Department of Geological Sciences and Geological Engineering, Queen's University, ON., Canada

ABSTRACT
This paper presents a grain-based discrete element model for simulating the quasi-brittle failure of rocks under mechanical loading. In this approach, the development of crack along grain boundaries controls the degree of damage in rock. A cohesive crack model based on the theory of "Non-linear Elastic Fracture Mechanics (NLEFM)" is implemented into the UDEC distinct element numerical code to define the constitutive behavior of the grain interfaces under different modes of fracturing. Implementation of the crack model in the grain-based simulator aims at enhancing the capability of the UDEC-Voronoi scheme to simulate the micro-cracking mechanisms more realistically similar the micro-cracking mechanisms. Rock heterogeneity, due to the presence of different mineral grains, is introduced to the model by considering the mineral composition of real rock and contrast in mechanical properties of the constituent minerals. The elastic properties of the grains and the strength properties at grain boundaries are extracted based on the experimental data. Then, the capability of the model to replicate the mechanical behavior of Lac du Bonnet (LDB) granite under compression and tension is evaluated. To do so, a series of uniaxial and triaxial compression and Brazilian tests is simulated. The mechanical response of the numerical models is found to be in good agreement with the response of the real rock observed in laboratory.

RÉSUMÉ
Cet article présente un modèle par éléments discrets basé sur l'échelle du grain pour modéliser la rupture quasi fragile de roches sous chargement mécanique. Dans cette approche, le développement de la fissure le long des joints de grains contrôle le degré d'endommagement de la roche. Un modèle de cohésion de fissure basé sur les théories de la «mécanique non-linéaire de la rupture (NLEFM)" est mis en œuvre dans le code numérique par élément distinct UDEC pour établir le comportement des interfaces des grains sous différents modes de fracturation. La mise en œuvre du modèle de fissuration dans le simulateur basé sur les grains vise à renforcer la capacité de l'approche UDEC-Voronoi à modéliser de façon plus réaliste les mécanismes de microfissuration. L'hétérogénéité de la roche, causée par la présence de grains de différente minéralogie, est introduite dans le modèle en prenant en compte la composition minérale de roche et le contraste des propriétés mécaniques des minéraux constituants. Les propriétés élastiques des grains et les propriétés de résistance aux joints des grains sont extraites de la base des données expérimentales. Ensuite, la capacité du modèle, à reproduire le comportement mécanique du granite du Lac du Bonnet en compression et en tension, est évaluée. Pour ce faire, une série d'essais de compression uniaxiaux, d'essais triaxiaux et d'essais Brésiliens est simulée. La réponse mécanique des modèles numériques se trouve à être en bon accord avec la réponse de la roche réelle observée en laboratoire.

1. INTRODUCTION

The process of brittle rock fracture during compression and tension is a result of the initiation, growth, and coalescence of multiple individual micro-cracks which eventually leads to formation of some clustered regions of macro-fractures in rock. As the compressive, or tensile stress applies across the boundaries of a rock sample, a complex heterogeneous stress system will be distributed through the rock in which the tensile and shear stresses will be concentrated at pre-existing flaws (i.e. micro-cracks, grain boundaries, cavities, cleavages) (Kranz, 1983). If the localized tensile stress exceeds the local strength of the microstructure some micro-cracks start to form at the point on the boundary of pre-existing flaw where tensile stress concentration is greatest. These axially aligned extensional micro-cracks occur during the early loading stages of compression tests. As the applied deviatoric stresses increase in the specimen, the density of compression-induced tensile cracks increases, and eventual interaction and coalescence of these cracks result in formation of some localized and macroscopic damaged zones in the material. It is the presence and creation of such micro-fractures that cause the compressional stress-strain curve of rock to deviate from true elastic (linearity) in the pre-failure region (Hazzard et al., 2000).

In this paper, a grain-based Discrete Element Method (DEM) is used for modelling the progression of damage during brittle fracturing of the crystalline rock. The key concept of explicit DEM is that the domain of interest is represented as an assemblage of dense packing rigid or deformable blocks/particles interacting together at their contact boundaries. In the other words, the model is composed of a series of particles that are glued together by their cohesive bonds forming between their boundaries. As a result, crack nucleation is simulated through breaking of internal bonds while fracture propagation is obtained by coalescence of multiple bond breakages.

In the DEM-Voronoi model the rock materials are represented by a pack of polygonal-shaped blocks. Owing to the full contact between grains and better interlocking offered by the random polygonal shapes, the Voronoi model overcomes some of the limitations of parallel-bonded particle models (Potyondy, 2012; Lisjak and Grasselli, 2014). In addition to that, it appears that polygonal structure used in UDEC compared to square and circular particles may be more representative of the mineral structure observed in crystalline rock (Lan et al., 2010; Lemos, 2001).

In DEM-Voronoi model, the behavior of the grains and their contact interfaces defines the macroscopic response of the rock, as the result, the success of models to reproduce the different aspects of brittle failure process relies on realistic description of constitutive laws assigned to constituents of the model. One important issue that should be considered in a gain-based model is to implement constitutive laws for behavior of the grains interfaces based on the concept of “Non-linear Fracture Mechanics (NLEFM)”. Implementing a “Cohesive Crack Model” to grains contacts allows to take into account the effects of material softening in front of the crack tip known as the “Fracture Process Zone (FPZ)” after the bond between two grains breaks and a new crack is formed.

The present paper aims to evaluate the capability of the grain-based DEM model to simulate fracturing of brittle rock when a Cohesive Crack Model is assigned to the interfaces forming between grain boundaries. The fundamental principles of implemented Cohesive Crack Models will be discussed. The micro-parameters of the model are calibrated to the macro experimental data reported for Lac du Bonnet granite.

2. GENERATION OF THE GRAIN-BASED MODEL

Calibration and simulations are based on the short-term laboratory properties of LDB granite sampled from 240m level at the Underground Research Laboratory in Pinawa, Canada. The model configurations for UCS test and Brazilan test are illustrated in Fig. 1, respectively. The grain-scale material heterogeneity is introduced to the model based on mineral composition of the LDB granite. Hence, four material grain types are defined, namely K-feldspar grain, Plagioclase grain, Quartz grain, and Biotite grain (Table. 1). The histogram in Fig. 2 compares the distribution of various mineral phases in both real granite and the UCS model.

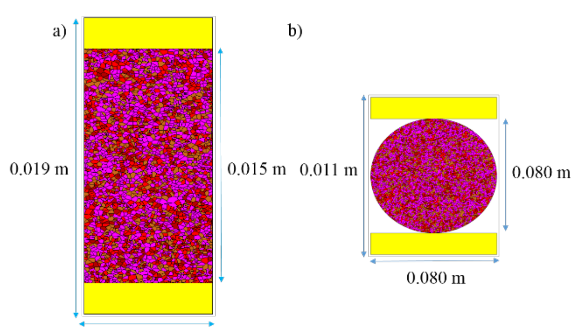

Fig. 1. Model geometry for (a) UCS testing; and (b) Brazilian testing. Grains with purple, light red, light brown, and dark red represent K-feldspar, plagioclase feldspar, quartz, and biotite minerals, respectively.

Table 1. Micro-material properties for different minerals of Lac du Bonnet.

Mineral phase	Alkali-feldspar	Plagioclase feldspar	Quartz	Biotite
Abundance	42%	22%	29%	6%
Grain size (mm)	3	3.5	1.5	0.75
Density (Kg/m^3)	2560	2630	2650	3050
Young's modulus (GPa)	69.8	88.1	94.5	33.8
Poisson's ratio (-)	0.28	0.26	0.08	0.36
Mode I fracture toughness, K_{IC} (MPa.$m^{0.5}$)	4.18 ± 0.09	4.18 ± 0.09	8.68 ± 0.18	3.21 ± 0.05

Values of Young's modulus for different minerals are given from Bass (1995).
Values of Young's modulus, density and Poisson's ratio for Quartz are given from Mavko et al. (2003).
Values of K_{IC} for different minerals are given from Mahabadi (2012).

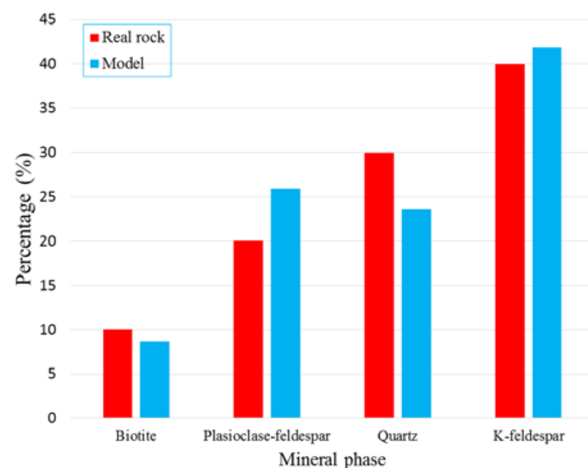

Fig. 2. Histogram showing the abundance of different mineral phases in real LDB granite and the SRM model.

3. COHESIVE CRACK MODEL DESCRIBING THE BEHAVIOR OF GRAIN CONTACTS

Experimental observation demonstrated during fracturing of quasi-brittle materials (Fig. 3) such as concrete and rock there is some intermediate space between cracked and uncracked portion of the material. This region which is forms at the tip of an opening (Mode I) crack defined as the Fracture Process Zone (FPZ). FPZ is a zone of partially damaged and interlocked material in which the damaged material is still able to withstand a stress and transfer load from one surface to the other (Fig. 4). The material outside the FPZ is assumed to be linear elastic (Dugdale, 1960; Hoagland et al., 1985; Labuz et al., 1985). As the crack propagates the micro-cracks in the FPZ merge and becomes a single structure to give continuity to the already existing crack. So indeed, FPZ acts as a bridging zone between cracked region and uncracked region.

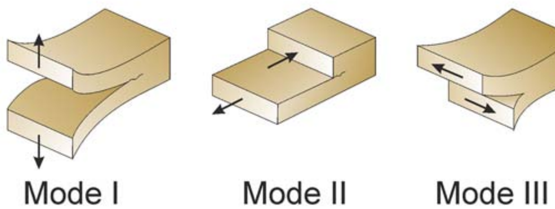

Fig. 3. Basics modes of fracturing. Any combination of these is referred to as mixed mode.

In an attempt to idealize the effect of the FPZ on fracturing of quasi-brittle materials several cohesive crack models for both Mode I (crack opening) and Mode II (crack sliding) have been proposed. The most important cohesive crack models (for idealization of Mode I fracturing) and slip-weakening models (for idealizing Mode II) are reported in Dugdale, 1960; Barenblatt, 1962; Hillerborg, 1976; Labuz et al., 1983) and in Ida, 1972; Palmer and Rice, 1973, respectively.

In this paper, the initiation and growth of the explicit micro-cracks are simulated by means of breakage of the bonds between the polygonal grains. Thus, arbitrary fracture trajectories are free to develop within the constraints imposed by the Voronoi blocks geometry. Depending on the local stress and relative contact wall displacements, the contact may yield under Mode I (tensile Mode), Mode II (sliding Mode) or mixed-Mode I – II conditions (Fig. 3). A cohesive crack model and a slip-weakening model define the behavior of the grain interfaces in Mode I and Mode II of fracturing.

To describe the strength of the contacts in Mode I and Mode II of fracturing a Coulomb slip criterion with tension cut-off, as presented in Fig. 5, are used. In Mode I (tension), the contact yields if the opening of the contact,u, reaches the critical value, u_p, corresponding to the tensile strength of the contact, f_t. Similarly, Mode II of fracturing initiates when the shear slip of the contact,s, exceeds the a critical value, s_p, corresponding to shear strength of the contact, f_{sh}, defined as

$$|f_{sh}| = c_c + \sigma_n . \tan(\varphi_c) \qquad [1]$$

Where c_c is the internal cohesion, φ_c is the intact material friction angle, and σ_n is the normal stress acting across the contact.

The stress-displacement curve for Mode I and Mode II conditions has a non-linear pre-peak branch and a softening branch (Fig. 6). The non-linear pre-yield branch is intended to represents the decay of stiffness in pre-failure state due to the progression of damage.

In the post-yield state (softening branch), the following stress-displacement (traction-separation) which links the cohesive stress transmitted by the contact to the contact displacement in tensile and shear states is used:

$$\begin{bmatrix}\sigma\\ \tau\end{bmatrix} = \chi(D_i).\begin{bmatrix}f_t\\ f_{sh}\end{bmatrix} \qquad [2]$$

Where f_t and f_{sh} are the strengths of contact in tension and shear, respectively, and $\chi(D)$ is softening function which defines the decay of contact strength in post-yield regions.

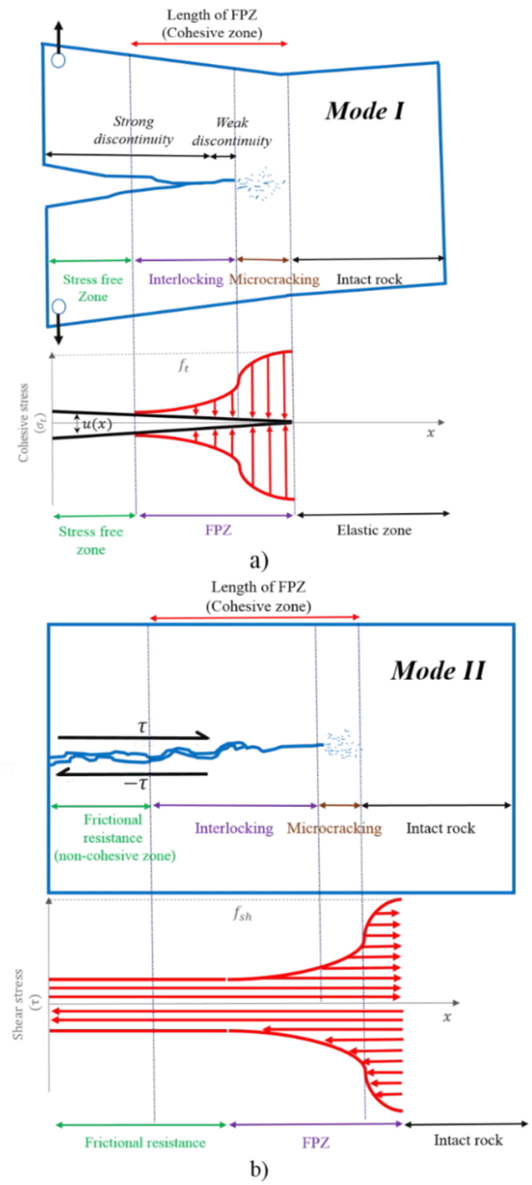

Fig. 4. Phenomenological description of a quasi-brittle fracturing process in (a) Mode I (Modified from Huespe and Oliver, 2011); (b) Mode II.

Based on a comprehensive analysis of experimental results reported by Evans and Marathe (1968), the following relation is proposed for a softening law

$$\chi(D_i) = \left[1 - \frac{A+B-1}{A+B} . \exp\left(D_i \frac{A+C\times B}{A+B(1-A-B)}\right)\right]. \qquad [3]$$
$$[A(1-D_i) + B(1-D_i)^C]$$

Where A, B, and C are empirical curve fitting parameters equal to 0.63, 1.8, and 6.0, respectively; and D_i $(i = I, II, I-II)$ is a damage variable with a value between 0 and 1. This equation defines the shape of the softening branch of the stress-displacement curves in both Mode I and Mode II of fracturing.

Thus, contact cohesive stress in Mode I and Mode II of fracturing are expressed in Eqs (4) and (5), respectively as

$$\sigma = \begin{cases} k_t.u.\ exp\left(-\dfrac{u}{u_p}\right) & u < u_p \\ \chi(D_I).f_t & u_p \le u < u_{res} \\ 0 & u \ge u_{res} \end{cases} \qquad [4]$$

$$\tau = \begin{cases} k_{sh}.s.\ exp\left(-\dfrac{s}{s_p}\right) & s < s_p \\ \chi(D_{II}).f_{sh} & s_p \le s < s_{res} \\ f_{res} & s \ge s_{res} \end{cases} \qquad [5]$$

Where u_p and s_p are values of normal and shear displacements at which contact undergoes yield in tension and shear, respectively. u_{res} and s_{res} are the residual opening and slippage in Mode I and Mode II conditions, respectively.

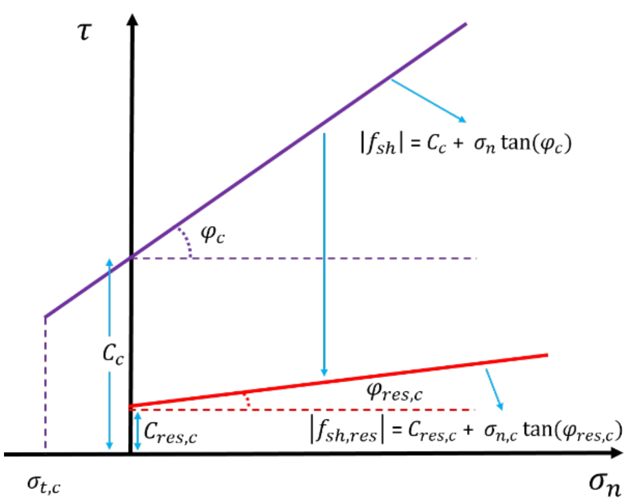

Fig. 5. Coulomb slip criterion with residual strength and tension cut-off to define the strength properties of the contacts in shear and tension.

The damage variable for contact subjected to Mode I (Mahabadi, 2012), Mode II, and mixed-Mode I–II (Tatone, 2014) displacements are defined, respectively, as

$$D_I = \frac{u - u_p}{u_{res} - u_p} \qquad [6]$$

$$D_{II} = \frac{s - s_p}{s_{res} - s_p} \qquad [7]$$

$$D_{I-II} = \sqrt{\left(\frac{u - u_p}{u_{res} - u_p}\right)^2 + \left(\frac{s - s_p}{s_{res} - s_p}\right)^2} \qquad [8]$$

Where u and s are the values of contact relative displacement in normal and shear directions, respectively.

Displacements at peak strength are evaluated as

$$u_p = e.\frac{f_t}{k_t} \qquad [9]$$

$$s_p = e.\frac{f_{sh}}{k_{sh}} \qquad [10]$$

Where $e = \exp(1) = 2.718281$ is the base of the natural logarithm.

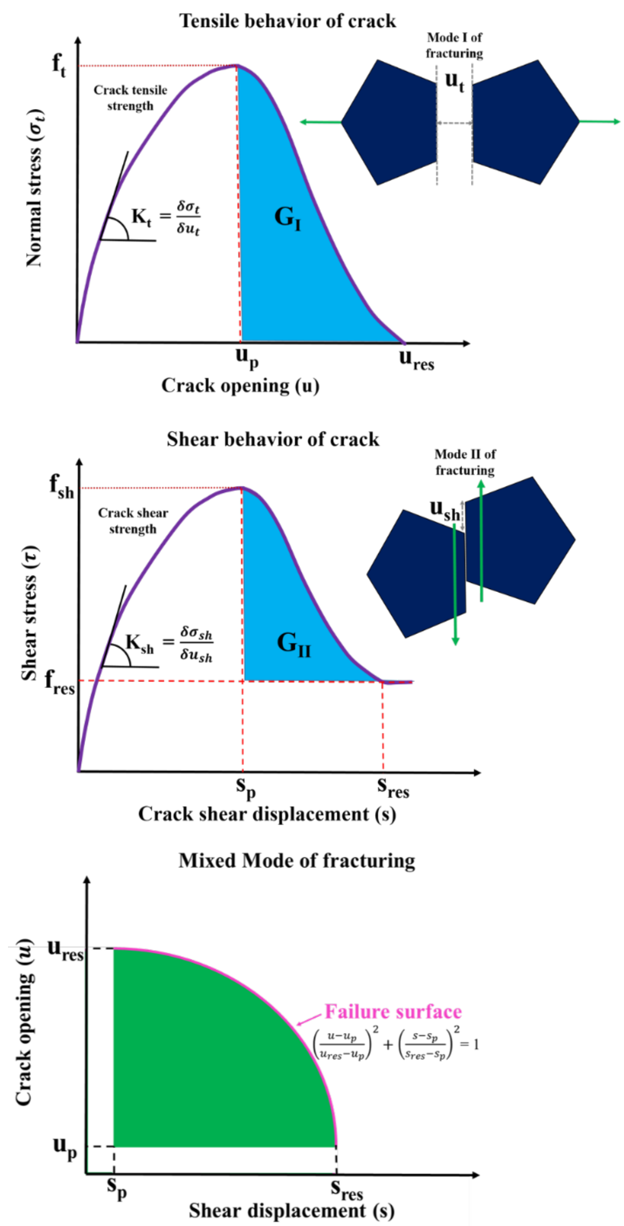

Fig. 6. Stress-displacement behavior of cohesive contact model in Mode I, Mode II, and mixed-Mode I-II.

The values of residual opening, u_{res} and slip, s_{res}, depends on the values of G_{Ic} and G_{IIc} of the Mode I and Mode II fracture energy release rates, f_t and f_{sh}. The values of G_{Ic} and G_{IIc} define as the energy that is required to extend the crack surface of a unit area. The areas under curves in Fig.6 (a) and (b) represent the energy needed to fully open the unit area of contact surface.

$$G_{Ic}=\int_{u_p}^{u_{res}} \chi(D_I).f_t\, du \quad [11]$$

$$G_{IIc}=\int_{s_p}^{s_{res}} [\chi(D_{II}).f_{sh} - f_{res}]\, ds \quad [12]$$

As a result, by solving the Eqs (11) and (12) the values of residual opening, u_{res} and slip, s_{res} are obtained as

$$u_{res} = u_p + \frac{3G_{Ic}}{f_t} \quad [13]$$

$$s_{res} = s_p + \frac{3G_{IIc}}{f_{sh}} \quad [14]$$

Based on the Griffith theory (1921), the value of G_{Ic} can be estimated as

$$G_{Ic} = \frac{K_{Ic}{}^2}{E} \quad [15]$$

Where K_{Ic} is fracture toughness of crack in Mode I, and E is Young's modulus of the material surrounding the crack. In this paper, the values of G_{IIc} is considered to be 2 times of G_{Ic}.

In order to model the non-linear behavior of contact under compressive normal stress (Fig. 7), the following hyperbolic function for normal closure of the contact with respect to normal stress as reported in Bandis et al. (1983) are used;

$$\sigma_n = \frac{k_{n0}\, u}{1-(u/u_{max})} \quad [16]$$

Where k_{n0} represents the initial normal stiffness of the contact, and u is the contact closure under compression, and u_{max} is the maximum possible contact closure.

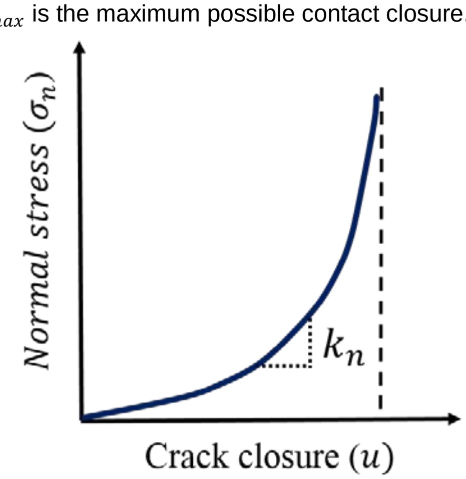

Fig. 7. Behavior of the contact under pure compression loading.

4. MODEL CALIBRATION

In order to calibrate the hydro-mechanical properties of the model, first the deformability (stiffness) of the UCS sample including elastic modulus and Poisson's ratio are calibrated to match those of the real rock. Afterwards, the micro-parameters of the sample will be corrected until the macro-response of the model mimics the tensile response of the rock in the Brazilian indirect tensile. And finally, the compressional peak strength and failure envelope properties of LDB granite will be calibrated (Farahmand and Diederichs, 2015).

In this study, the following relation is used to determine the normal stiffness of the contacts:

$$k_{n,c} = \text{n} \;.\; max\left(\frac{K+\left(\frac{4}{3}\right)G}{\Delta Z_{min}}\right),\ 1 \le n \le 10 \quad [17]$$

Where n is a multiplier factor, K and G are the bulk and shear moduli, respectively; and ΔZ_{min} is the smallest width of adjoining zone in the normal direction. The value of $k_{sh,c}$ is also can be obtained using $\frac{k_{sh,c}}{k_{n,c}} = \frac{G}{E}$ relation.

After assigning the density and the elastic properties of the grains, the value for $k_{n,c}$ should be adjusted until the macroscopic Young's modulus of the model matches the target value. Diederichs (2000) showed that for the material Poisson's ratio in BPM models is related to the proportion of contact hear stiffness to normal stiffness ($\frac{k_{sh,c}}{k_{n,c}}$). As this stiffness ratio decreases, Poisson's ratio increases and the sample becomes more dilatant. The value for initial aperture of the contacts are calibrated such that the permeability of the sample match that of the real rock in the non-stressed condition. Then, the value of the calibrated residual aperture are finded by performing a series of compressive hydro-mechanical tests in the way that the permeability of the model in elastic portion of axial stress-strain curve match permeability of LDB granite at the corresponding stress state (Farahmand and Diederichs 2014). The values for tensile strength of different mineral interfaces are taken from the results of laboratory testing on different mineral samples reported in Savanick and Johnson (1974). As Brazilian test and UCS test result in lower macroscopic tensile and crack initiation threshold, the contact tensile strength extracted from Savanick and Johnson (1974) are increased until the correct indirect tensile strength and crack initiation stress are obtained. Initially the value of contact cohesion should be selected in order to reproduce target unconfined peak strength. In this study, initially cohesion value for each type of the contacts is set to four times of the contact tensile strength ($\frac{c_c}{\sigma_{t,c}}$ = 4) based on the results reported by Laqueche et al. (1986) and Okubo and Fukui (1996). The friction angle of contacts are calibrated by conducting a series of triaxial compression tests with different confining pressure.

5. BOUNADARY CONDITIONS

To load the sample in uniaxial and triaxial boundary conditions, the rock sample is subjected to a constant displacement rate to induce stresses until failure is achieved. To do this, the rock is located between two extremely stiff platens with thickness of 20 mm and 15 mm for UCS and Brazilian samples, respectively. The upper and lower platens move towards each other to apply load on two ends of the rock. In the case of biaxial loading, confining stresses corresponding to minor principal stress (σ_3) are exerted on the external lateral sides of the model.

Since the solution algorithm of the UDEC is dynamics and is based on timestepping, the rate of loading applying on platens must be defined. However, high loading rates or platens velocities result in numerical oscillations within the sample, it is important that the velocity of converging platens be such that perturbations can be dissipated throughout the sample faster than new loads and displacements are applied

To avoid numerical instability in the model, the loading rate in compressional tests should be applied in the way that in each timestep the quasi-static equilibrium satisfies. This prevents the stress delay occurring between two ends of the specimen. As Kazerani et al. (2012) suggested, the loading process is divided into a set of stages. During each stage, the platens converges by the velocities of 0.02 m/s and 0.01 m/s for the case of UCS and Brazilian test, respectively. Then, the loading is stopped by setting the platens velocities to zero, and then the model is cycled until quasi-static equilibrium for the system is reached.

6. CALIBRATION RESULTS

Since the models are composed of four different mineral phases, ten contact types as listed in Table. 2 are needed to be calibrated. Fig. 8. represents the ten interfaces types in a part of the model.

Table 2. Type of the interfaces in the models based on contacts forming between different mineral grains.

Mineral phase	K-feldspar	Plagioclase feldspar	Quartz	Biotite
K-feldspar	1	2	3	4
Plagioclase feldspar		5	6	7
Quartz			8	9
Biotite				10

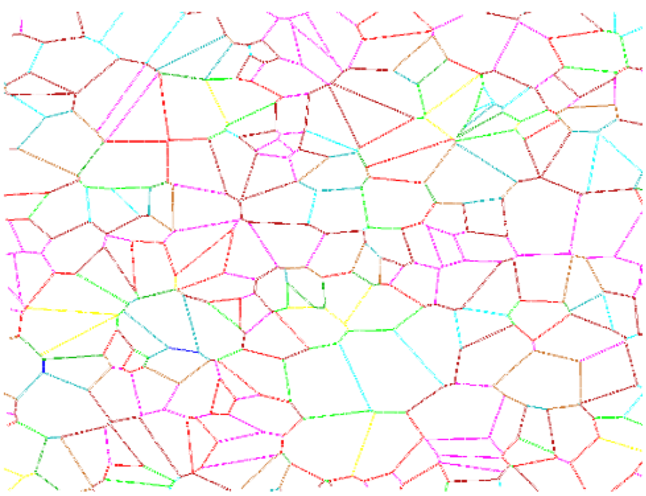

represented by different colour. See Table 2 for a list of the interface types.

Calibrated contact properties for defined 10 various interfaces of the model are given in Table 3. Figs 10 and 11 show the resultant stress – strain curve of the Brazilian and unconfined compression tests, respectively. Obtained strength properties of the model such as tensile strength, compressive peak strength, crack damage, and crack initiation thresholds demonstrate a very good agreement with those of the experimental data.

The axial stress – axial strain response of the model in compression deviates from linearity at $\sigma_1 = 181$ MPa (87% of UCS), which is corresponds to the reversal point in volumetric –strain – axial strain curve. While the onset of crack initiation occurs at 86 MPa, which is determined based on the onset of tensile cracking in the model (red lines in Fig. 11 (a)). The crack initiation stress occurs approximately at 41% of the UCS. These results compare very closely to the experimental response in which the Crack Initiation and Crack Damage stresses occurs at 41% and 86% 0f the peak strength, respectively (Table. 4). The number of induced cracks demonstrates that the primary mechanism of damage in the model is extensile cracking, while the shear (cohesive) cracking starts to become the dominant only after the stress in the sample reaches the Crack Damage threshold. Summary of the experimental and simulated results are given in Table 4.

Table 3. Calibrated micro properties for contacts.

Interface ID	$\sigma_{t,c}$ (MPa)	$\sigma_{res,t,c}$ (MPa)	c_c (MPa)	$c_{res,c}$ (MPa)	φ_c (^{0})	$\varphi_{res,c}$ (^{0})	$K_{n,c}$ (GPa/m)	$k_{sh,c}/k_{n,c}$
1	35.0	0	110	0	62	5	230000	0.65
2	32.0	0	108	0	61	5	210000	0.65
3	28.2	0	76	0	53	5	270000	0.65
4	11.4	0	60	0	48	5	230000	0.65
5	37.0	0	112	0	63	5	250000	0.65
6	28.2	0	80	0	49	5	230000	0.65
7	22.4	0	54	0	45	5	230000	0.65
8	35.0	0	130	0	65	5	280000	0.65
9	23.4	0	57	0	52	5	230000	0.65
10	25.3	0	88	0	55	5	130000	0.65

Under unconfined compressive loading condition, accumulation of damage in the direction sub-parallel to applied loading axis creates macroscopic fracture patterns in form of axial splitting (Fig. 11 (b)). In case in which the rock is under indirect tensile load, the corresponding fracture patterns are in form of some extensile cracks which extends from top to bottom of the model (Fig. 10). These fracture patterns are in good agreement with those typically observed in the laboratory (Horii and Nemat-Nasser, 1986).

The strength envelope were obtained by performing a set of biaxial tests at three different confining pressure. The results of rupture strength of the rock at different confining stresses are used to derive the Mohr-Coulomb properties of the rock. The strength envelopes exhibited approximately a linear relationship for confinement higher than zero for the range of confining stresses applied ($0 \le \sigma_3 \le 15$ MPa). Obtained cohesion and friction angle for specimens match very closely with laboratory date reported by Martin (1993) as the simulated cohesion and friction angle were found as 29.3 MPa and 58.9°, with 2.33% and 1.35% errors compared to the experimental values, respectively.

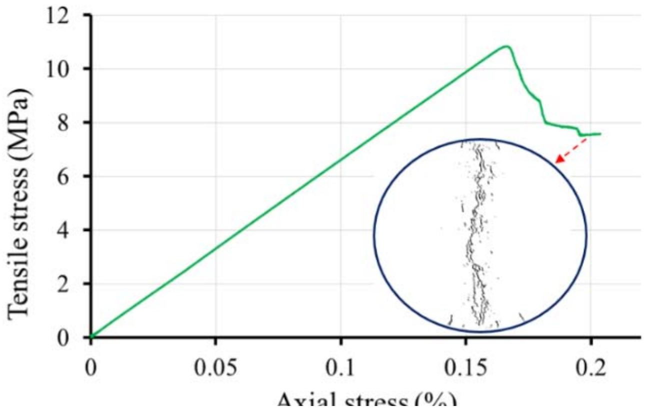

Fig. 10. Tensile stress – Axial strain curve obtained from calibrated Brazilian model.

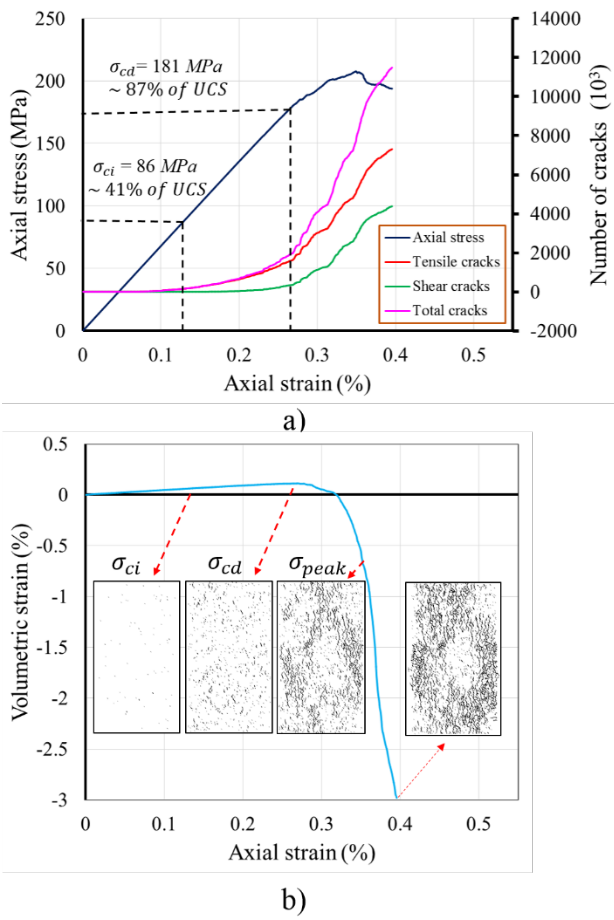

Fig. 11. Model response during uniaxial compression test; a) axial stress – axial strain curve and associated incremental accumulation of tensile (extension) cracks and shear (cohesive) cracks. b) volumetric strain – axial strain curve.

Table 4. Comparison between experimental and simulation results for LDB granite (Values of experimental data are given from Martin (1993).

Property	Experimental	Model
Young's modulus (GPa)	69 $\pm$5.8 (n = 81)	67.9
Poisson's ratio (−)	0.26 $\pm$0.04 (n = 81)	0.26
Tensile strength (MPa)	9.3 $\pm$1.3 (n = 39)	10.8
UCS(MPa)	200 $\pm$22 (n = 81)	207
Crack initiation stress (MPa)	90 + σ_3, $\sigma_3 <$ 30 (41% of UCS)	86 (41% of UCS)
Crack damage stress (MPa)	172, $\sigma_3 = 0$ (86% of UCS)	181 (87% of UCS)
Friction angle(degree)	59	58.2
Cohesion (MPa)	30	29.3

7. CONCLUSIONS

A heterogeneous grain-based model for simulating the response of Lac du Bonnet during tension and compression is presented. A cohesive crack model based on the theories of "Non-linear Fracture Mechanics (NLEFM)" is implemented into the UDEC distinct element numerical code to define the constitutive behavior of the grain interfaces under different modes of fracturing. A calibration process aims to find values of micro-parameters of the model that can reproduce the macro properties of the rock are discussed. The ability of the calibrated model to reproduce different aspects of mechanical behavior of the brittle rock is examined.

The numerical experimentations demonstrate the capability of discrete element-Voronoi model to mimic the pre- and post-failure response of brittle materials. The calibrated model very accurately predicts, in a quantitative sense, the macroscopic properties of real granite such as elastic properties, damage thresholds (crack initiation and interaction stresses), peak strength (tensile and compression strengths), triaxial strength envelope (friction angle and cohesion).

8. REFERENCES

Bandis, S. C., Lumsden, A. C., & Barton, N. R. 1983. Fundamentals of rock joint deformation. In *International Journal of Rock Mechanics and Mining Sciences & Geomechanics Abstracts* (Vol. 20, No. 6, pp. 249-268). Pergamon.

Bass, D. j. 1995. Elasticity of minerals, glasses and melts. In *Mineral Physics and crystallography, Ref. Shelf Ser.*, vol. 2, edited by T. J. Ahrens, pp. 45-63, AGU, Washington, D. C.

Barenblatt, G. I. 1962. The mathematical theory of equilibrium cracks in brittle fracture. *Advances in applied mechanics*, *7*(55-129), 104.

Diederichs, M.S. 2000. Instability of hard rockmasses: the role of tensile damage and relaxation. *Ph.D. thesis, University of Waterloo.* P. 566.

Dugdale, D. S. 1960. Yielding of steel sheets containing slits. *Journal of the Mechanics and Physics of Solids*, *8*(2), 100-104.

Evans, R. H., & Marathe, M. S. (1968). Microcracking and stress-strain curves for concrete in tension. *Materials and Structures*, *1*(1), 61-64.

Farahmand, K., Diederichs, M.S. 2015. A calibrated Synthetic Rock Mass (SRM) model for simulating crack growth in granitic rock considering grain scale heterogeneity of polycrystalline rock. In Proceedings of *49th US Rock Mechanics/Geomechanics Symposium*. American Rock Mechanics Association.

Griffith, A. A. 1921. The phenomena of rupture and flow in solids. *Philosophical transactions of the royal society of london. Series A, containing papers of a mathematical or physical character*, 163-198.

Hazzard, J. F., Young, R. P., & Maxwell, S. C. 2000. Micromechanical modeling of cracking and failure in brittle rocks. *Journal of Geophysical Research: Solid Earth (1978–2012)*, *105*(B7), 16683-16697.

Hillerborg, A., Modéer, M., & Petersson, P. E. 1976. Analysis of crack formation and crack growth in concrete by means of fracture mechanics and finite elements. *Cement and concrete research*, *6*(6), 773-781.

Hoagland, R. G., Hahn, G. T., & Rosenfield, A. R. 1973. Influence of microstructure on fracture propagation in rock. *Rock Mechanics*, *5*(2), 77-106.

Horii, H., & Nemat-Nasser, S. 1986. Brittle failure in compression: splitting, faulting and brittle-ductile transition. *Philosophical Transactions of the Royal Society of London. Series A, Mathematical and Physical Sciences*, *319*(1549), 337-374.

Huespe, A. E., & Oliver, J. 2011. *Crack models with embedded discontinuities* (pp. 99-159). Springer Vienna.

Itasca Consulting Group Inc., 2014. UDEC (universal distinct element code). Minneapolis, USA: Itasca Consulting Group Inc.

Ida, Y. 1972. Cohesive force across the tip of a longitudinal-shear crack and Griffith's specific surface energy. *Journal of Geophysical Research*, *77*(20), 3796-3805.

Kranz, R. L. 1983. Microcracks in rocks: a review. *Tectonophysics*, *100*(1), 449-480.

Kazerani, T., Yang, Z. Y., & Zhao, J. 2012. A discrete element model for predicting shear strength and degradation of rock joint by using compressive and tensile test data. *Rock mechanics and rock engineering*, *45*(5), 695-709.

Labuz J. F., Shah S. P. and Dowding C. H. 1983. Post peak tensile load-displacement response and the fracture process zone in rock, Proc. 24th U.S. Symposium on Rock Mechanics, pp. 421-428. College Station, Texas.

Labuz, J. F., Shah, S. P., & Dowding, C. H. 1985. Experimental analysis of crack propagation in granite. In *International Journal of Rock Mechanics and Mining Sciences & Geomechanics Abstracts* (Vol. 22, No. 2, pp. 85-98). Pergamon.

Lan, H., Martin, C. D., & Hu, B. 2010. Effect of heterogeneity of brittle rock on micromechanical extensile behavior during compression loading. *Journal of Geophysical Research: Solid Earth (1978–2012)*, *115*(B1).

Laqueche, H., Rousseau, A., & Valentin, G. 1986. Crack propagation under Mode I and II loading in slate schist. In *International Journal of Rock Mechanics and Mining Sciences & Geomechanics Abstracts* (Vol. 23, No. 5, pp. 347-354). Pergamon.

Lemos JV. 2001. Recent development and future trends in distinct element methods – UDEC/3DEC and PFC codes. In: *Zhao j, Ohnishi Y, Zhao G, Sasaki T, editors. Advances in Discontinuous Numerical Methods and Applications in Geomechanics and Geoengineering.* London: Tylor & Francis Group; 2012.

Lisjak, A., & Grasselli, G. 2014. A review of discrete modeling techniques for fracturing processes in discontinuous rock masses. *Journal of Rock Mechanics and Geotechnical Engineering*, *6*(4), 301-314.

Mahabadi, O. K. 2012. Investigating the influence of micro-scale heterogeneity and microstructure on the failure and mechanical behaviour of geomaterials. *PhD thesis, University of Toronto*.

Martin CD. 1993. The strength of massive Lac du Bonnet granite around underground openings. *Ph.D thesis, University of Manitoba, Winnipeg, Canada*.

Mavko, G., Mukerji, T. & Dvorkin, J. 2003. The rock physics hand book: Tools for seismic analysis of porous media. *Cambridge University Press*, New York.

Okubo, S., & Fukui, K. 1996. Complete stress-strain curves for various rock types in uniaxial tension. In *International Journal of Rock Mechanics and Mining Sciences & Geomechanics Abstracts* (Vol. 33, No. 6, pp. 549-556). Pergamon.

Palmer, A. C., & Rice, J. R. 1973. The growth of slip surfaces in the progressive failure of over-consolidated clay. *Proceedings of the Royal Society of London. A. Mathematical and Physical Sciences*, *332*(1591), 527-548.

Potyondy, D. O. 2012. A flat-jointed bonded-particle material for hard rock. In *Proceedings of 46th US rock mechanics/geomechanics symposium (ARMA), Chicago*, Paper 12-501.

Savanick, G. A., & Johnson, D. I. 1974. Measurements of the strength of grain boundaries in rock. In *International Journal of Rock Mechanics and Mining Sciences & Geomechanics Abstracts* (Vol. 11, No. 5, pp. 173-180). Pergamon.

Tatone, S. A. B. (2014). *Investigating the evolution of rock discontinuity asperity degradation and void space morphology under direct shear* (Doctoral dissertation).